Journal of Electroanalytical Chemistry xxx (2010) xxx–xxx

Contents lists available at ScienceDirect

Journal of Electroanalytical Chemistry

journal homepage: www.elsevier.com/locate/jelechem

Analysis of the hydrogen electrode reaction mechanism in thin-layer cells. 1. Theory

José L. Fernández *

Programa de Electroquímica Aplicada e Ingeniería Electroquímica (PRELINE), Facultad de Ingeniería Química, Universidad Nacional del Litoral, Santiago del Estero 2829, (S3000AOM) Santa Fe, Argentina

ARTICLE INFO

Article history:
Received 14 April 2010
Received in revised form 30 June 2010
Accepted 1 September 2010
Available online xxxx

Keywords:
Thin-layer cell
Hydrogen
Electrocatalysis
SECM

ABSTRACT

This work develops the equations that relate the kinetic parameters of the hydrogen electrode reaction (HER) with the current density (j) vs. potential (E) dependences of a thin-layer cell (TLC). Two operation modes of the TLC are analyzed. The first one proposes to examine the $j(E)$ dependence of the hydrogen evolution reaction (*her*) on one electrode while the paired electrode oxidized the dissolved H_2 back to H^+ under diffusion control. The second mode proposes to analyze the $j(E)$ dependence of the hydrogen oxidation reaction (*hor*) on one electrode while the other generates dissolved H_2 from H^+ under diffusion control. In both cases, as very high mass-transport rates are reached for distances in the micrometer range, the $j(E)$ curves are sensitive to the complete set of kinetic parameters even for very large reaction rates. Possible ways to incorporate these equations in the theoretical formalisms of well-established TLC-based techniques such as scanning electrochemical microscopy are discussed.

1. Introduction

The hydrogen electrode reaction (HER) in acid medium, Eq. (1), operates through the Volmer–Heyrovsky–Tafel (VHT) mechanism, which is represented by Eqs. (2)–(4), where S denotes an active site. It proceeds via two parallel pathways, which are the Volmer–Tafel (VT) and the Volmer–Heyrovsky (VH) routes [1].

$$H^+ + e^- \rightleftarrows \frac{1}{2}H_{2(g)} \quad (1)$$

$$H^+ + S + e^- \rightleftarrows S{-}H_{(a)} \quad \text{Volmer} \quad (2)$$

$$H^+ + S{-}H_{(a)} + e^- \rightleftarrows H_{2(g)} + S \quad \text{Heyrovsky} \quad (3)$$

$$S{-}H_{(a)} + S{-}H_{(a)} \rightleftarrows H_{2(g)} + 2\,S \quad \text{Tafel} \quad (4)$$

The relative weights of these routes on the reaction rate at each potential are established according to the values of the elementary kinetic parameters. Thus, the current density (j) vs. potential (E) dependence could be dominated primarily by just one of these routes over a certain potential range, and by the other in a different range [2,3]. In this context, for interpretation of $j(E)$ curves it is important to use a kinetic model that takes into account the possible occurrence of both routes [4,5]. Moreover, likewise important is to analyze experimental data from the reaction operating under activated control over a wide range of potential, so that the route transition can be readily observed [6,7]. On the basis of a rigorous treatment of the VHT mechanism, Chialvo and co-workers developed the kinetic equations that describe the complete steady-state $j(E)$ dependence for the HER [8]. They were able to reproduce the $j(E)$ dependences of a Pt rotating disk electrode (RDE) for the hydrogen oxidation reaction (*hor*), the hydrogen evolution reaction (*her*), and around the equilibrium potential, with a single set of elementary kinetic parameters. The importance of working in conditions of high mass-transport rates for accurate determination of all kinetic parameters of the HER was remarked by these authors [3,8,9].

The configuration of a thin-layer cell (TLC) operating in steady state allows to reach very high mass-transport rates by approaching two electrodes to micro- and sub-micrometer distances [10]. Even though the first TLC experiments were reported more than four decades ago [10–12], there is a renewed interest in this configuration. This interest is raised by novel electrochemical techniques that exploit the recent progresses in nanopositioning and nanofabrication to create TLCs with submicron separations. Such are the cases, for example, of the scanning electrochemical microscopy (SECM) [13] and of the nanofluidic channels [14].

This work presents the analysis of two possible ways to study the mechanism of the HER in acid medium in conditions of high mass-transport rates using TLC-based techniques. Both the *her* and the *hor* are analyzed in two different TLC configurations, and the VHT mechanism is solved for both cases without aprioristic restrictions about rate-determining steps.

* Tel.: +54 342 4571164x2519.
E-mail address: jlfernan@fiq.unl.edu.ar

1572-6657/$ - see front matter © 2010 Elsevier B.V. All rights reserved.
doi:10.1016/j.jelechem.2010.09.002

2. Theory

2.1. Basic equations for the HER

From a mass balance of the reaction defined by Eq. (1) operating in steady state through the VHT mechanism, the following relationships between the reaction rate (V) and the elementary step rates (v_i) are obtained.

$$V = v_V + v_H = 2(v_V - v_T) = 2(v_H + v_T) \tag{5}$$

The elementary step rates can be written in terms of the electrode potential referred to the reversible hydrogen electrode (RHE) potential (E_{RHE}) according to Eqs. (6)–(8) [4], where $\eta = E - E_{RHE}$. The RHE is defined at the proton concentration of the solution ($c^*_{H^+}$) and at a hydrogen pressure (p_{H2}) of 1 atm.

$$v_V = v_V^e\left[\left(\frac{1-\theta(\eta)}{1-\theta^e}\right)C^s_{H^+}e^{-(1-\alpha)f\eta} - \left(\frac{\theta(\eta)}{\theta^e}\right)e^{\alpha f\eta}\right] \tag{6}$$

$$v_H = v_H^e\left[\left(\frac{\theta(\eta)}{\theta^e}\right)C^s_{H^+}e^{-(1-\alpha)f\eta} - \left(\frac{1-\theta(\eta)}{1-\theta^e}\right)\left(\frac{C^s_{H_2}}{C^*_{H_2}}\right)e^{\alpha f\eta}\right] \tag{7}$$

$$v_T = v_T^e\left[\left(\frac{\theta(\eta)}{\theta^e}\right)^2 - \left(\frac{C^s_{H_2}}{C^*_{H_2}}\right)\left(\frac{1-\theta(\eta)}{1-\theta^e}\right)^2\right] \tag{8}$$

In these equations, θ and θ^e are the adsorbed-H coverages evaluated at E and at E_{RHE}, respectively, α is the symmetry factor (considered equal for both steps), and $f = F/RT$ (F is the Faraday constant, R is the gas constant and T is temperature). The terms C^s_i are surface concentrations normalized respect to $c^*_{H^+}$, and $C^*_{H_2} = c^*_{H_2}/c^*_{H^+}$, where $c^*_{H_2}$ is the concentration of dissolved H_2 in the RHE (i.e. $c^*_{H_2} = 9.1 \times 10^{-7}$ mol cm^{-3} in 10 mM H_2SO_4 for $p_{H_2} = 1$ atm [15]). A Langmuir-type model was adopted for the adsorbed-H intermediate. Besides, v_i^e are the equilibrium elementary step rates evaluated in the conditions of the RHE. These parameters are related with the reaction-rate constants of each elementary step ($k_{\pm i}$) by Eqs. (9)–(11) [16].

$$v_V^e = \frac{k_{+V}\left(c^*_{H^+}\right)^{\alpha}}{1 + \left(\frac{k_{+T}}{k_{-T}}\right)^{-1/2}} \tag{9}$$

$$v_H^e = \frac{k_{+H}\left(c^*_{H^+}\right)^{\alpha}}{1 + \left(\frac{k_{+T}}{k_{-T}}\right)^{1/2}} \tag{10}$$

$$v_T^e = \frac{k_{+T}}{\left[1 + \left(\frac{k_{+T}}{k_{-T}}\right)^{-1/2}\right]^2} \tag{11}$$

2.2. Basic steady-state TLC equations

The general equations for a TLC operating in steady state have been previously derived [10]. The specific situation that is the focus of this work is represented in Scheme 1. The system is a four-electrode cell with two working electrodes (1 and 2) separated a distance d. The potentials of both electrodes (η_1 and η_2) are independently controlled respect to the RHE. Initially there is no dissolved H_2 in the cell solution. Fick's Laws are solved in one dimension (x) for the steady-state diffusion of H^+ and electrogenerated H_2 between both electrodes. At open circuit, or null TLC current density, the concentrations of H^+ ($c^{oc}_{H^+}$) and dissolved H_2 ($c^{oc}_{H_2}$) are constant and equal to their initial values ($c^*_{H^+}$ and 0, respectively). At certain η_1 and η_2 values, the steady-state fluxes (J) of H^+ and dissolved H_2 are constant. They are related between them

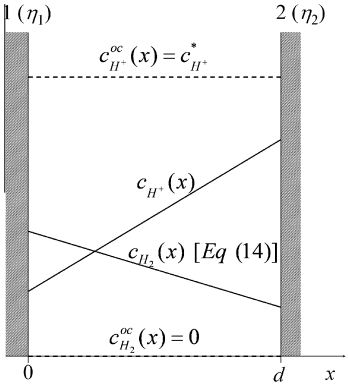

Scheme 1. Diagram of the two-electrode thin-layer cell for studying the HER.

and with the current density by Eq. (12). Note that the current densities of electrodes 1 and 2, j_1 and j_2 respectively, have opposite signs since both electrodes have facing surfaces.

$$J_{H^+}(\eta_1,\eta_2) = -2J_{H_2}(\eta_1,\eta_2) = -\frac{j_1(\eta_1,\eta_2)}{F} = \frac{j_2(\eta_1,\eta_2)}{F} \tag{12}$$

Thus, taking into account the Fick's first law, the steady-state concentration profiles result linear with x and are given by Eqs. (13) and (14). In these equations, D_i are the diffusion coefficients and x_o is a reference coordinate, for example where c_{H^+} is fixed.

$$c_{H^+}(x) = c_{H^+}(x_o) + \frac{j_1}{FD_{H^+}}(x - x_o) \tag{13}$$

$$c_{H_2}(x) = c_{H_2}(x_o) - \frac{j_1}{2FD_{H_2}}(x - x_o) = \left(\frac{D_{H^+}}{2D_{H_2}}\right)\left[c^*_{H^+} - c_{H^+}(x)\right] \tag{14}$$

2.3. The her in a TLC

The experiment setup that is proposed to study the *her* in a TLC is represented in Scheme 2a. The *her* is studied on electrode 1, which potential (η_1) is varied over a range where H^+ reduction occurs. Electrode 2 operates at a positive enough potential where electrogenerated dissolved H_2 is oxidized back to H^+ at diffusion-limiting rate. In this case, as the electrode 2 holds the value of $c_{H^+}(d)$ in $c^*_{H^+}$, the thickness of the diffusion layer is controlled by the distance between both electrodes. Taking into account the boundary conditions and the reaction-rate expressions (see Appendix A), the three equivalent dependences of the current density of electrode 1 on η_1 given by Eq. (15) are obtained.

$$\begin{aligned} j_1 &= \frac{v_V^e\left[\left(\frac{1-\theta(\eta_1)}{1-\theta^e}\right)e^{-f\eta_1} - \left(\frac{\theta(\eta_1)}{\theta^e}\right)\right] + v_H^e\left(\frac{\theta(\eta_1)}{\theta^e}\right)e^{-f\eta_1}}{\frac{e^{-\alpha f\eta_1}}{F} + \left\{v_V^e\left(\frac{1-\theta(\eta_1)}{1-\theta^e}\right)e^{-f\eta_1} + v_H^e\left[\left(\frac{\theta(\eta_1)}{\theta^e}\right)e^{-f\eta_1} - \xi\left(\frac{1-\theta(\eta_1)}{1-\theta^e}\right)\right]\right\}\frac{1}{j_L}} \\ &= \frac{v_V^e\left[\left(\frac{1-\theta(\eta_1)}{1-\theta^e}\right)e^{-f\eta_1} - \left(\frac{\theta(\eta_1)}{\theta^e}\right)\right] - v_T^e\left(\frac{\theta(\eta_1)}{\theta^e}\right)^2}{\frac{1}{2F} + \left[v_V^e\left(\frac{1-\theta(\eta_1)}{1-\theta^e}\right)e^{-(1-\alpha)f\eta_1} - v_T^e\xi\left(\frac{1-\theta(\eta_1)}{1-\theta^e}\right)^2\right]\frac{1}{j_L}} \\ &= \frac{\left(\frac{\theta(\eta_1)}{\theta^e}\right)\left[v_H^e e^{-(1-\alpha)f\eta_1} + v_T^e\left(\frac{\theta(\eta_1)}{\theta^e}\right)\right]}{\frac{1}{2F} + \left\{v_H^e\left[\left(\frac{\theta(\eta_1)}{\theta^e}\right)e^{-f\eta_1} + \xi\left(\frac{1-\theta(\eta_1)}{1-\theta^e}\right)\right]e^{\alpha f\eta_1} + v_T^e\xi\left(\frac{1-\theta(\eta_1)}{1-\theta^e}\right)^2\right\}\frac{1}{j_L}} \end{aligned} \tag{15}$$

The parameter ξ groups the diffusion coefficients and concentrations of H^+ and H_2 in the RHE according to Eq. (16). Moreover, Eq. (17) gives the diffusion-limiting TLC current density (j_L), which is obtained when $C_{H^+}(x = 0) \cong 0$ and $C_{H_2}(x = d) = 0$.

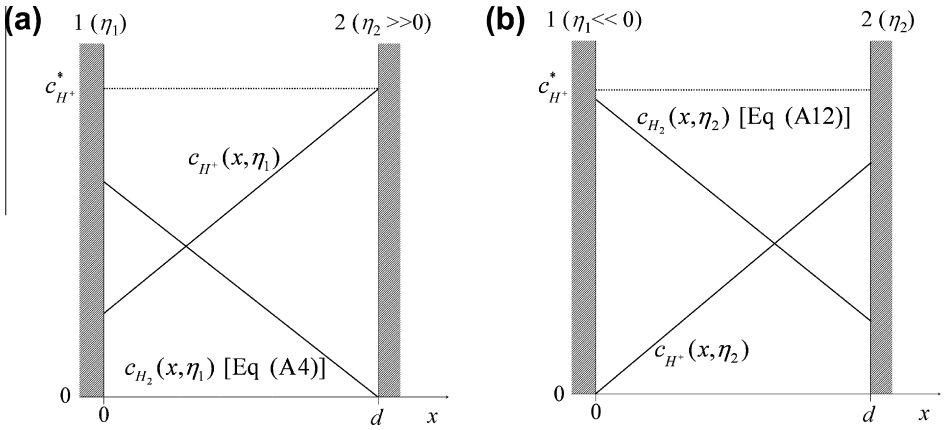

Scheme 2. Diagrams of the TLC configurations for studying the *her* on electrode 1 (a) and the *hor* on electrode 2 (b).

$$\xi = \left(\frac{D_{H^+}}{2D_{H_2}}\right)\left(\frac{c^*_{H^+}}{c^*_{H_2}}\right) \tag{16}$$

$$j_L = \frac{FD_{H^+}c^*_{H^+}}{d} \tag{17}$$

Besides, $\theta(\eta_1)$ is a third-order polynomial function of η_1 that can be obtained, for instance, rearranging the last equality in Eq. (15). As it was demonstrated in previous works [17] as η_1 tends to very negative values, θ approaches to a limiting value (θ^*), which could be different to one depending on the elementary kinetic parameters and on j_L.

On the other hand, when the *her* is infinitely fast the mass-transport controlled (reversible) current density should be defined by Eq. (18), which can be obtained from the Nernst equation (see Appendix A).

$$j_1 = \frac{j_L}{2}\left[\xi e^{2f\eta_1} + 2 - \sqrt{(\xi e^{2f\eta_1}+2)^2 - 4}\right] \tag{18}$$

2.4. The hor in a TLC

The electrode setup for studying the *hor* in a TLC is represented in Scheme 2b. Electrode 1 operates at a negative enough potential where H^+ is reduced to H_2 at diffusion-limiting rate. The *hor* is studied on electrode 2, which potential (η_2) is varied over a range where dissolved H_2 diffusing from the surface of electrode 1 is oxidized to H^+. The current density at electrode 1 is used for the analysis since it is sensitive to the H^+ feedback. Taking into account the boundary conditions and the reaction-rate expressions (see Appendix A), the three equivalent dependences of the current density of electrode 1 on η_2 given by Eq. (19) are obtained. Again, ξ and j_L are defined by Eqs. (16) and (17), respectively.

$$\begin{aligned} j_1 &= \frac{v^e_V\left(\frac{\theta(\eta_2)}{\theta^e}\right) + v^e_H\xi\left(\frac{1-\theta(\eta_2)}{1-\theta^e}\right)}{\frac{e^{-\alpha f\eta_2}}{F} + \left\{v^e_V\left(\frac{1-\theta(\eta_2)}{1-\theta^e}\right)e^{-f\eta_2} + v^e_H\left[\left(\frac{\theta(\eta_2)}{\theta^e}\right)e^{-f\eta_2} - \xi\left(\frac{1-\theta(\eta_2)}{1-\theta^e}\right)\right]\right\}\frac{1}{j_L}} \\ &= \frac{v^e_V\left(\frac{\theta(\eta_2)}{\theta^e}\right)e^{\alpha f\eta_2} + v^e_T\left[\left(\frac{\theta(\eta_2)}{\theta^e}\right)^2 - \xi\left(\frac{1-\theta(\eta_2)}{1-\theta^e}\right)^2\right]}{\frac{1}{2F} + \left[v^e_V\left(\frac{1-\theta(\eta_2)}{1-\theta^e}\right)e^{-(1-\alpha)f\eta_2} - v^e_T\xi\left(\frac{1-\theta(\eta_2)}{1-\theta^e}\right)^2\right]\frac{1}{j_L}} \\ &= \frac{v^e_H\xi\left(\frac{1-\theta(\eta_2)}{1-\theta^e}\right)e^{\alpha f\eta_2} - v^e_T\left[\left(\frac{\theta(\eta_2)}{\theta^e}\right)^2 - \xi\left(\frac{1-\theta(\eta_2)}{1-\theta^e}\right)^2\right]}{\frac{1}{2F} + \left\{v^e_H\left[\left(\frac{\theta(\eta_2)}{\theta^e}\right)e^{-f\eta_2} + \xi\left(\frac{1-\theta(\eta_2)}{1-\theta^e}\right)\right]e^{\alpha f\eta_2} + v^e_T\xi\left(\frac{1-\theta(\eta_2)}{1-\theta^e}\right)^2\right\}\frac{1}{j_L}} \end{aligned} \tag{19}$$

Similarly to the previous case, θ is a cubic function of η_2 that can be obtained, for instance, reorganizing the last equality in Eq. (19). On the other hand, Eq. (20) gives the mass-transport controlled $j_1(\eta_2)$ dependence expected for the *hor* operating with an infinitely large reaction rate (see Appendix A).

$$j_1 = \frac{j_L}{2}\left[\sqrt{\xi e^{2f\eta_2}(\xi e^{2f\eta_2}+4)} - \xi e^{2f\eta_2}\right] \tag{20}$$

3. Discussion

3.1. General remarks

Two important issues related to the kinetic model and to the reactant and product concentrations should be remarked. On the one hand, in these treatments the adsorption of atomic hydrogen intermediate follows a Langmuir-type model. Surely a more complex model that takes into account the interaction between adsorbed species, such as Frumkin, should be more realistic. This is particularly critical for modeling the *her* when precise calculations of kinetic parameters are required [18]. However, the simpler Langmuir assumption is a good first approximation for the analysis of the descriptive capabilities of the derived equations.

On the other hand, it should be noted that on a proton-reducing electrode operating under mass-transport limiting condition, the concentration of H^+ at the electrode surface is negligible, but not null. In fact, as water is a source of protons, at negative enough potentials the current for hydrogen evolution should increase due to water dissociation [19]. Thus, a diffusion-limiting current for proton reduction is only established over a potential window where the surface concentration of H^+ is very small and the water discharge is negligible. As expected, the extension of this potential window depends on the solution pH (or $c^*_{H^+}$).

3.2. The HER in a TLC

The HER proceeds via two parallel pathways, which are the Volmer–Tafel and the Volmer–Heyrovsky routes. Thus, it is interesting to analyze how the interplay of these routes affects the $j_1(\eta, d)$ dependences for selected sets of kinetic parameters, both for the *her* and for the *hor*.

In the first TLC configuration, the approach of an electrode to a surface that keeps the reactant concentration at the bulk value produces a decrease of the diffusion-layer thickness with the consequent increase of the mass-transport rate. Such property is exploited, e.g. using SECM in the nanometer scale [20] and

nanofluidic channels [14], to measure rate constants of fast single-step electrode reactions such as the ferrocene electro-oxidation. In the case of a multistep reaction such as the *her*, increasing the mass-transport rate affects the $j(\eta)$ dependence according to the kinetic parameters of the elementary steps. Thus, in order to evaluate the effect of d on the $j_1(\eta_1)$ dependences, these were simulated with Eq. (15) using different equilibrium reaction rates, coverage values, and distances. A typical situation was supposed with a concentration of protons $c^*_{H^+} = 0.02$ M, which is low enough to prevent nucleation of H_2 bubbles [21]. In these conditions, assuming diffusion coefficient values of $D_{H^+} = 7.1 \times 10^{-5}$ cm^2 s^{-1} [21] and $D_{H2} = 1.4 \times 10^{-5}$ cm^2 s^{-1} [15], a value of $\xi = 55.73$ is calculated. From the derived equations for $c_{H_2}(d)$, it is obvious that the concentration of dissolved hydrogen can take values as large as $\xi c^*_{H_2}$. This means that, in the supposed conditions, the dissolved-hydrogen concentration overpasses the saturation value for 1 atm by almost two orders of magnitude. In spite of this, it is an experimental observation that H_2 bubbles are not nucleated as long as $c^*_{H^+} < 0.06$ M [21], which is well explained by the supersaturation of dissolved H_2 at the electrode surface [22].

A group of $j_1(\eta_1)$ dependences for the *her* that were simulated using quite large equilibrium rates (in the order of those measured on Pt [8]) and different d values are shown in Fig. 1. These curves are normalized respect to the corresponding j_L values calculated using Eq. (17). The $j_1(\eta_1)$ dependence for a reversible reaction (dashed line) and those simulated using the same kinetic parameters but $v^e_H = 0$, which correspond to just the Volmer–Tafel route (j^{VT}, dotted lines), were also plotted. The resulting $\theta(\eta_1)$ dependences are shown in a separate graph. From the analysis of these *her* curves it is concluded that, for these kinetic parameters typical of a good catalyst such as Pt, at distances larger than 10 μm the *her* operates under mass-transport control (reversible). For distances in the range $d < 10$ μm, there is an increase of the limiting current density that brings the electrode operation into a mixed control. As long as $d \geqslant 0.3$ μm the $j_1(\eta_1)$ curves are mainly dominated by the VT route before the coverage reaches a limiting value, which is lesser than one ($\theta^* < 1$), and the current arrives at the diffusion limiting value (j_L). This is verified when comparing the $j_1(\eta_1)$ curves with the corresponding $j^{VT}(\eta_1)$ dependences. It is observed that there are no significant differences between the $j_1(\eta_1)$ and the $j^{VT}(\eta_1)$ dependences for $d \geqslant 0.3$ μm. Thus, the $j_1(\eta_1)$ curve is not sensitive to the VH route under these conditions. As j_L becomes larger for $d < 0.3$ μm, the $j_1(\eta_1)$ dependence shows an inflexion (or shoulder). For a better understanding of this behavior it is useful to analyze only the VT route, which tends to reach a kinetic limiting rate. This limiting value, which is observed in the $j^{VT}(\eta_1)$ curves, is established when the H-coverage reaches a limiting value. The *her* Volmer–Tafel limiting current density ($j_L^{VT,her}$) value depends on the kinetic parameters and on j_L according to Eq. (15) evaluated for $v^e_H = 0$, $\eta \to -\infty$, and $\theta = \theta^*$, which leads to Eq. (21)

$$j_L^{VT,her} = \frac{2F v_T^e \left(\frac{\theta^*}{\theta^e}\right)^2}{1 + \frac{2F v_T^e \xi}{j_L}\left(\frac{1-\theta^*}{1-\theta^e}\right)^2} \tag{21}$$

The dependence of θ^* and of $j_L^{VT,her}$ on d (or j_L) is plotted in Fig. 2 for different values of v^e_T. For a certain value of v^e_T, there is a domain of distances where $\theta^* \cong 1$ and $j_L^{VT,her} = 2F v_T^e (\theta^e)^{-2} < j_L$. As v^e_T becomes larger, this domain shifts to smaller d values. For example, for the parameters used in the simulated curves of Fig. 1, curve (b) in Fig. 2II shows that $j_L^{VT,her} \cong j_L$ ($\theta^* < 1$) as long as $d \geqslant 0.3$ μm, and deviates from j_L when d becomes smaller than 0.3 μm ($j_L > 4.5$ A cm^{-2}). At more negative potentials the VH route becomes relevant (in detriment of the VT route) and raises the current density until it reaches the diffusion limiting value. As a consequence, a shoulder is verified in the $j_1(\eta_1)$ response, which highlights the transition from the VT route to VH route. Such inflexion is only evident when $v^e_H \ll v^e_T$ and the j_L values are large enough to make $j_L^{VT,her} < j_L$ (>4.5 A cm^{-2} or $d < 0.3$ μm for the kinetic parameters used in Fig. 1).

On the other hand, the second TLC configuration, which resembles the feedback mode of SECM, permits to study the kinetics of a reaction on electrode 2 by measuring feedback current in electrode 1. In other words, the $j_1(\eta_2)$ dependence is analyzed. This configuration was proved to be quite practical for localized kinetic studies on macroelectrodes using SECM [23,24], and was applied in a few studies of the *hor* on varied materials [21,25–27]. High mass-transport rates are reached by fixing the concentration of the electrode-two reactant (H_2) at its maximum value on the electrode-one surface and approaching both electrodes to submicron distances. The feedback current is affected by the reaction rate at electrode 2, and so by the kinetic parameters. To evaluate this effect for the case of the *hor*, simulations of the $j_1(\eta_2)$ dependences were carried out with Eq. (19). On this sense, Fig. 3 shows the normalized

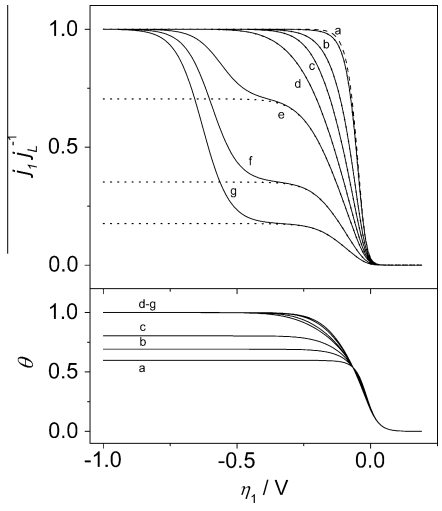

Fig. 1. Dependences of the normalized current density of electrode 1 for the *her* and of the adsorbed-H coverage (θ) on the potential of electrode 1 (solid lines), calculated using Eq. (15). Equilibrium rates (mol s^{-1} cm^{-2}): $v^e_V = 10^{-5}$, $v^e_H = 10^{-10}$, $v^e_T = 10^{-6}$. $\theta^e = 0.2$. $\alpha = 0.5$. d (μm) = 10 (a), 1 (b), 0.5 (c), 0.3 (d), 0.2 (e), 0.1 (f), 0.05 (g). Dotted lines are the dependences for the VT route calculated using the same parameters but $v^e_H = 0$. Dashed line is the reversible dependence calculated using Eq. (18).

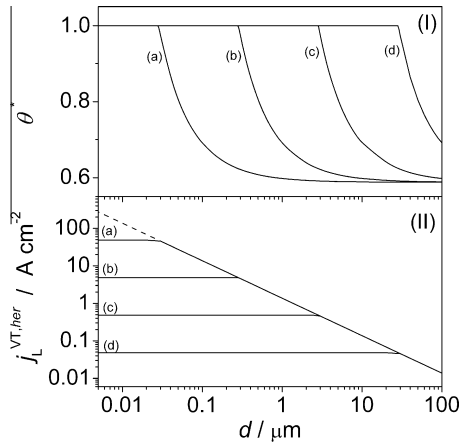

Fig. 2. Dependences on the electrode distance of the limiting coverage of adsorbed H (I) and of the normalized VT limiting current density (II). Equilibrium rates (mol s^{-1} cm^{-2}): $v^e_V = 10^{-5}$, $v^e_H = 0$, $v^e_T = 10^{-5}$ (a), 10^{-6} (b), 10^{-7} (c), 10^{-8} (d). $\theta^e = 0.2$. $\alpha = 0.5$. Dashed line is the dependence $j_L(d)$ according to Eq. (17).

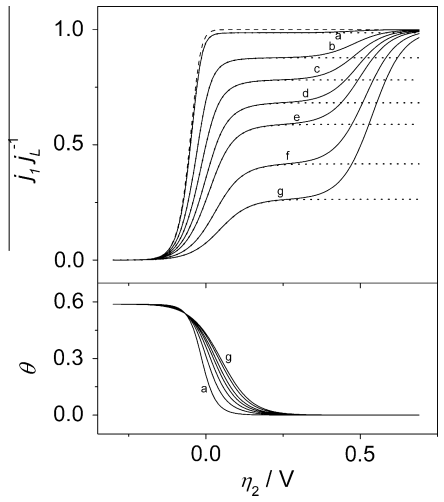

Fig. 3. Dependences of the normalized current density of electrode 1 for the *hor* and of the adsorbed-H coverage (θ) on the potential of electrode 2 (solid lines), calculated using Eq. (19). Parameters are as in Fig. 1. Dotted lines are the dependences of the VT route calculated using $v_H^e = 0$. Dashed line is the reversible dependence calculated using Eq. (20).

$j_1(\eta_2)$ dependences for the *hor* obtained with the same kinetic parameters and distances as those used in Fig. 1. The dependences for a reversible reaction (dashed lines) and for the Volmer–Tafel route simulated with $v_H^e = 0$ (dotted lines), were also plotted. The resulting θ (η_2) dependences are included in a separate graph. The analysis of these simulated *hor* curves leads to basically the same conclusions as those drawn for the *her*. The reaction looks reversible at distances larger than 10 μm. However, differently to the *her*, a *hor* Volmer–Tafel limiting current density ($j_L^{VT,hor}$) separates from the j_L value already from $d \leqslant 10$ μm ($j_L > 0.1$ A cm^{-2}). This VT limiting current is established when θ is null but $C_{H_2}^s$ is not, and was experimentally detected in a few studies of the *hor* on Pt ultramicroelectrodes (UMEs) [3,6,7] and ensembles of UMEs [2]. Similarly to the *her*, the $j_L^{VT,hor}$ value depends on the kinetic parameters and on j_L, in this case according to Eq. (22), which is obtained from Eq. (19) evaluated for $v_H^e = 0$ and $\theta = 0$. From this equation it is evident that, for the values $v_T^e = 10^{-6}$ mol s^{-1} cm^{-2} and $\theta^e = 0.2$ used in Fig. 3, $j_L^{VT,hor} < j_L$ only when $d \leqslant 10$ μm ($j_L \geqslant 0.14$ A cm^{-2}). As the potential increases ($\eta_2 > 0.2$ V for these parameters), the VH route starts to dominate the $j_1(\eta_2)$ dependence before it reaches the mass-transport limiting value.

$$\frac{1}{j_L^{VT,hor}} = \frac{1}{j_L} + \frac{(1-\theta^e)^2}{2F\xi v_T^e} \tag{22}$$

The potential value where from the VH-route rate becomes significant depends on the relative value of v_H^e respect to v_T^e. Thus for example, Fig. 4 shows that for v_H^e only two orders of magnitude smaller than v_T^e the current plateaus observed in both the $j_1(\eta_1)$ and $j_1(\eta_2)$ dependences extends over much narrower potential ranges. Moreover, Fig. 5 shows that for similar values of v_H^e and v_T^e, no shoulder is observed in the $j_1(\eta)$ curves. Besides, these last curves are only sensitive to the VH route, as can be verified when comparing them with the $j^{VH}(\eta)$ dependences simulated using $v_T^e = 0$ (dotted lines). For smaller v_H^e and v_T^e values like those used in the curves of Fig. 6, which could be typical of less active catalysts such as Au, the $j(\eta)$ curves present features distinctive of both routes only when j_L is not very large (or $d > 1$ μm). For large j_L values the VT contribution becomes imperceptible and the $j_1(\eta)$ curves show the typical behavior of an irreversible reaction. It is also interesting to analyze the effect of θ^e on the $j_1(\eta)$ curves in conditions of high j_L values, which can be observed in Fig. 7 for a set of large equilibrium rates. It is observed that for the analyzed kinetic parameters the $j_1(\eta)$ curves are quite sensitive to the θ^e value in the range $\theta^e \geqslant 0.1$.

3.3. First approaches for applications in SECM studies

The presented models can be used to study the *her* and the *hor* in experimental configurations that produce a TLC geometry. One of these configurations is the scanning electrochemical microscope, in which a disk-shaped UME tip with radius a (electrode 1) is approached to a substrate surface (electrode 2) and a TLC is established in the tip-substrate gap [28]. In the so-called feedback mode, the tip current is used to analyze an electrochemical reaction occurring either on the tip surface or on the substrate surface [23].

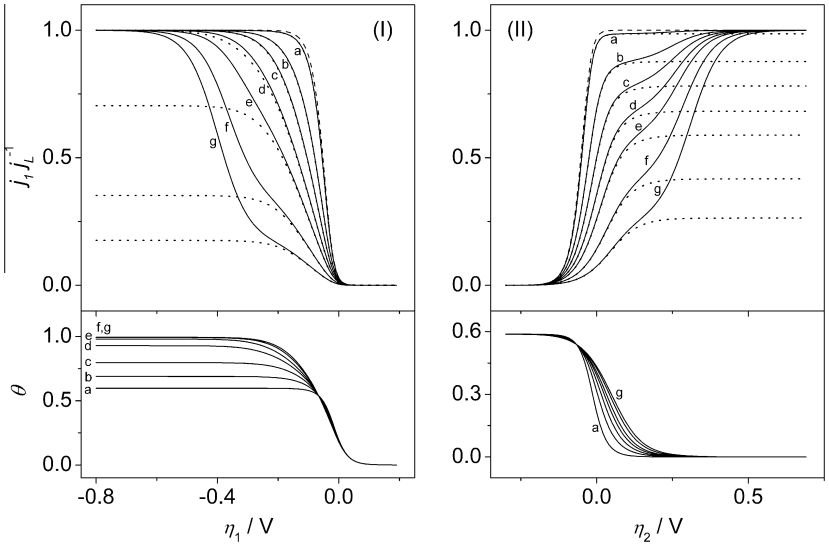

Fig. 4. Dependences of the normalized current density of electrode 1 and of the corresponding adsorbed-H coverages (θ) (solid lines) for the *her* on η_1 calculated with Eq. (15) (I) and for the *hor* on η_2 calculated with Eq. (19) (II). Equilibrium rates (mol s^{-1} cm^{-2}): $v_V^e = 10^{-5}$, $v_H^e = 10^{-8}$, $v_T^e = 10^{-6}$. $\theta^e = 0.2$. $\alpha = 0.5$. d (μm) = 10 (a), 1 (b), 0.5 (c), 0.3 (d), 0.2 (e), 0.1 (f), 0.05 (g). Dotted lines are the dependences for the VT route calculated with $v_H^e = 0$. Dashed lines are the reversible dependences calculated using Eqs. (18) and (20), respectively.

Please cite this article in press as: J.L. Fernández, J. Electroanal. Chem. (2010), doi:10.1016/j.jelechem.2010.09.002

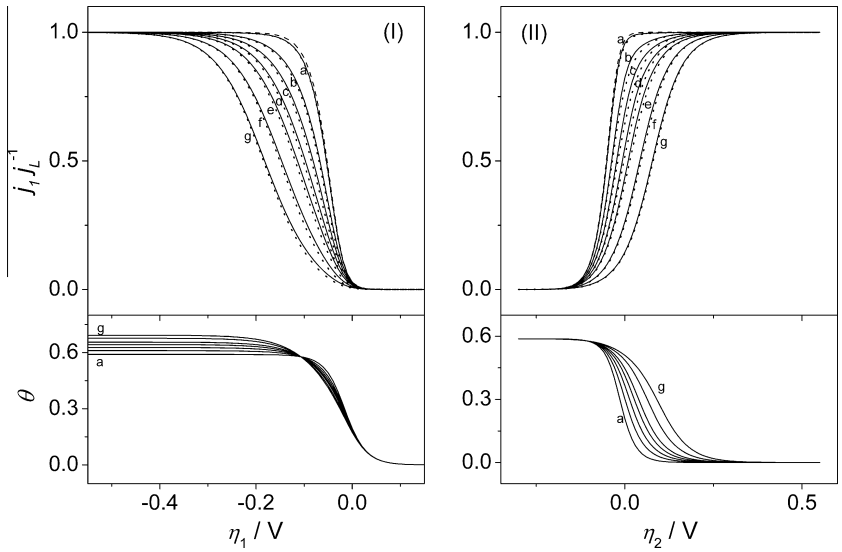

Fig. 5. Idem Fig. 4 but $v_H^e = 10^{-6}$ mol s^{-1} cm^{-2}. Dotted lines are the dependences for the VH route calculated with $v_T^e = 0$.

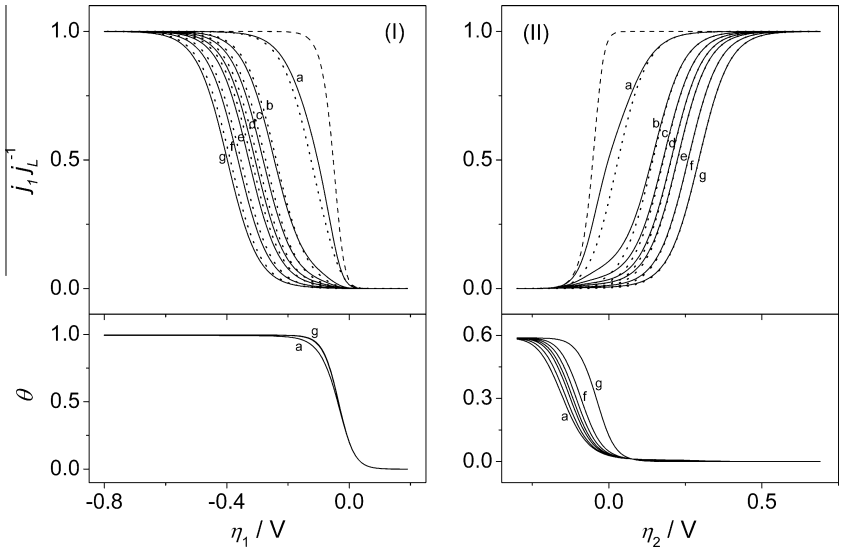

Fig. 6. Idem Fig. 4 but $v_T^e = 10^{-8}$ mol s^{-1} cm^{-2}. Dotted lines are the dependences for the VH route calculated with $v_T^e = 0$.

On the one hand, the *her* on a SECM tip can be analyzed using Eq. (23), which is an approximate analytical dependence of the tip current (I_T) on the tip-substrate distance (d) [29].

$$I_T(\eta_T, d) = I_{TLC}(\eta_T, d) + I_{T,\infty}(\eta_T) f_T(d) \tag{23}$$

Eq. (15) should be employed to take into account the dependence of the TLC current (I_{TLC}) on the tip potential (η_T) and on d. Moreover, to use Eq. (23) it is necessary to solve the VHT mechanism on a disk UME and find the dependence of the tip current at infinite distance ($I_{T,\infty}$) on η_T. The term $f_T(d)$ takes into account the blocking of diffusion toward the UME by the substrate surface at a specific d. It has the general form given by Eq. (24), whose parameters (A, C and D) are well known and depend on the overall tip dimensions [30]

$$f_T(d) = A + C \exp\left[\frac{D}{(d/a)}\right] \tag{24}$$

On the other hand, the analysis of the *hor* on a portion of an infinite SECM substrate could be performed using the dependence of the tip current on d and on the substrate potential (η_S) defined by

$$I_T(\eta_S, d) = I_{TLC}(\eta_S, d) + I_{T,L}(d, t) f_T(d) \tag{25}$$

This includes the TLC current, which can be calculated with Eq. (19). However, the analysis over the full potential range requires the modeling of the shielding of H^+ concentration due to consumption at the substrate at slightly negative η_S values [31,32]. So far a first approximation could be done by calculating the diffusion limiting tip current ($I_{T,L}$) with Eq. (26), using the local concentration of H^+ that results when solving the linear diffusion from the substrate. In these conditions of planar semi-infinite diffusion, the tip current only reaches a quasi-steady state at long times. Probably, a simpler and steady-state equation could be used when this analysis is performed on a substrate with size equal or smaller than the tip size.

$$I_{T,L} = 4FD_{H^+} c_{H^+}(d, t) a \tag{26}$$

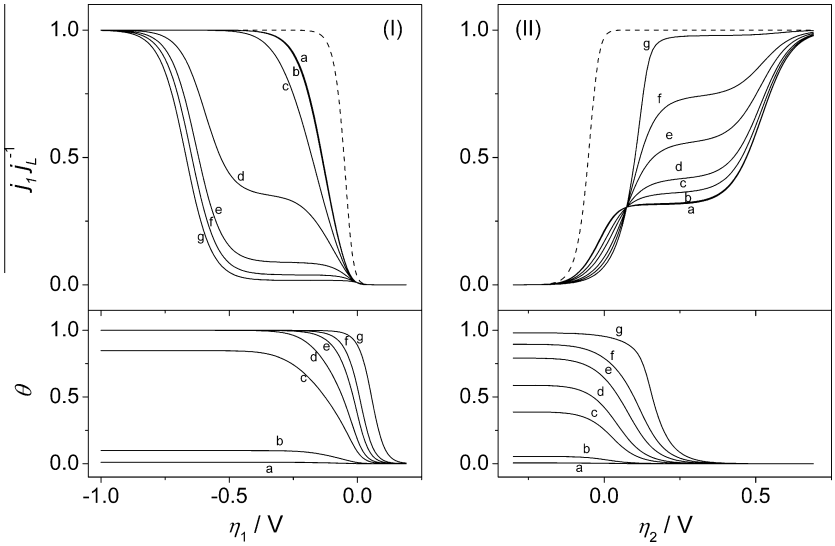

Fig. 7. Dependences of the normalized current density of electrode 1 and of the corresponding adsorbed-H coverages (θ) (solid lines) for the *her* on η_1 calculated with Eq. (15) (I) and for the *hor* on η_2 calculated with Eq. (19) (II). Equilibrium rates (mol s^{-1} cm^{-2}): $v_V^e = 10^{-5}$, $v_H^e = 10^{-10}$, $v_T^e = 10^{-6}$. d (μm) = 0.1. $\alpha = 0.5$. $\theta^e = 0.001$ (a), 0.01 (b), 0.1 (c), 0.2 (d), 0.4 (e), 0.6 (f), 0.9 (g). Dashed lines are the reversible dependences calculated using Eqs. (18) and (20), respectively.

4. Conclusions

Steady-state experiments in thin-layer cells can provide very useful mechanistic information of both the cathodic branch (the *her*) and the anodic branch (the *hor*) of the hydrogen electrode reaction. When the TLC distance is below 10 μm, the expected $j(\eta)$ responses are kinetically controlled even for the largest kinetic parameters known so far (as those reported for Pt). Thus, this technique is particularly useful to study the HER on highly active materials without mass-transport limitations. One of the most interesting properties verified from the presented theoretical analysis is the ability to highlight different mechanistic aspects of the reaction by manipulation of the electrode distance (d). On that sense, depending on the kinetic parameters and on d, the resulting $j(\eta)$ curves may be dominated by only one of the two possible mechanistic routes, or may reveal the simultaneous contributions and interactions of both routes. Nowadays there are techniques, such as SECM, that can establish a TLC with variable separation below 10 μm. By a proper inclusion of the developed models in the theoretical formalisms of these techniques, they surely will constitute powerful tools for determination of the complete set of HER kinetic parameters.

Acknowledgements

This work was supported by Agencia Nacional de Promoción Científica y Tecnológica (ANPCyT), Consejo Nacional de Investigaciones Científicas y Técnicas (CONICET) and Universidad Nacional del Litoral.

Appendix A

This appendix gives details on the derivation of Eqs. (15), (18), (19), and (20).

Derivation of Eq. (15). For the TLC operating to study the *her* according to Scheme 2a, the normalized concentrations of H^+ and H_2 at the electrode-two surface ($x = d$) are given by Eqs. (A1) and (A2). Moreover, from Eqs. (13) and (14), and taking into account that in this case $x_o = d$, the dependences $C_{H^+}(x)$ and $C_{H_2}(x)$ given by Eqs. (A3) and (A4) are obtained.

$$C_{H^+}(x = d) = 1 \tag{A1}$$

$$C_{H_2}(x = d) = 0 \tag{A2}$$

$$C_{H^+}(x) = 1 + \frac{j_1}{FD_{H^+}c^*_{H^+}}(x - d) \tag{A3}$$

$$C_{H_2}(x) = -\frac{j_1}{2FD_{H_2}c^*_{H^+}}(x - d) = \left(\frac{D_{H^+}}{2D_{H_2}}\right)[1 - C_{H^+}(x)] \tag{A4}$$

The normalized concentrations at the surface of electrode 1, that result when Eqs. (A3) and (A4) are evaluated at $x = 0$, are defined by

$$C^s_{H^+} = 1 - \frac{j_1}{FD_{H^+}c^*_{H^+}}d \tag{A5}$$

$$C^s_{H_2} = \frac{j_1}{2FD_{H_2}c^*_{H^+}}d = \left(\frac{D_{H^+}}{2D_{H_2}}\right)(1 - C^s_{H^+}) \tag{A6}$$

By substituting Eqs. (A5) and (A6) into Eqs. (6)–(8), the elementary reaction rates in terms of j_1 can be obtained. By replacing them into Eq. (5), taking into account that $V = j_1/F$ and rearranging, three independent equivalent dependences of j_1 vs. η_1 given by Eq. (15) are obtained.

Derivation of Eq. (18). The Nernst equation for the HER can be written in terms of the normalized surface concentrations according to the first equality in Eq. (A7). By substituting Eqs. (A5), (A6), (16), and (17), the dependence $j_1(\eta_1)$ given by the third term of Eq. (A7) is obtained.

$$e^{2f\eta_1} = \frac{C^{s2}_{H^+}}{C^s_{H_2}}\left(\frac{c^*_{H_2}}{c^*_{H^+}}\right) = \frac{(1 - j_1/j_L)^2}{\xi(j_1/j_L)} \tag{A7}$$

By reordering Eq. (A7), the second-order polynomial expression given by Eq. (A8) is obtained, which root can be calculated with Eq. (18).

$$j_1^2 - j_L(\xi e^{2f\eta_1} + 2)j_1 + j_L^2 = 0 \tag{A8}$$

Derivation of Eq. (19). For the TLC operating to study the *hor* according to Scheme 2b, the normalized concentrations of H^+ and H_2 at the electrode 1 surface ($x = 0$) are given by Eqs. (A9) and (A10). Moreover, from Eqs. (13) and (14), and taking into account

that in this case $x_o = 0$, the dependences $C_{H^+}(x)$ and $C_{H_2}(x)$ given by Eqs. (A11) and (A12) are obtained.

$$C_{H^+}(x=0) = 0 \tag{A9}$$

$$C_{H_2}(x=0) = \left(\frac{D_{H^+}}{2D_{H_2}}\right) \tag{A10}$$

$$C_{H^+}(x) = \frac{j_1}{FD_{H^+}c^*_{H^+}}x \tag{A11}$$

$$C_{H_2}(x) = \left(\frac{D_{H^+}}{2D_{H_2}}\right)\left(1 - \frac{j_1}{FD_{H^+}c^*_{H^+}}x\right) = \left(\frac{D_{H^+}}{2D_{H_2}}\right)[1 - C_{H^+}(x)] \tag{A12}$$

The normalized concentrations at the surface of electrode 2, that result when Eqs. (A11) and (A12) are evaluated at $x = d$, are defined by

$$C^s_{H^+} = \frac{j_1}{FD_{H^+}c^*_{H^+}}d \tag{A13}$$

$$C^s_{H_2} = \left(\frac{D_{H^+}}{2D_{H_2}}\right)\left(1 - \frac{j_1}{FD_{H^+}c^*_{H^+}}d\right) = \left(\frac{D_{H^+}}{2D_{H_2}}\right)(1 - C^s_{H^+}) \tag{A14}$$

By substituting Eqs. (A13) and (A14) into Eqs. (6)–(8), the elementary reaction rates in terms of j_1 can be obtained. By replacing them into Eq. (5), taking into account that $V = j_2/F = -j_1/F$, and rearranging terms, three independent dependences of j_1 vs. η_2 given by Eq. (19) are obtained.

Derivation of Eq. (20). By substituting Eqs. (A13), (A14), (16), and (17) in the Nernst equation for the HER, the dependence $j_1(\eta_2)$ given by Eq. (A15) is obtained

$$e^{2f\eta_2} = \frac{C^{s2}_{H^+}}{C^s_{H_2}}\left(\frac{c^*_{H_2}}{c^{*2}_{H^+}}\right) = \frac{(j_1/j_L)^2}{\xi(1 - j_1/j_L)} \tag{A15}$$

This can be reordered to a second-order polynomial expression given by Eq. (A16), which root can be calculated with Eq. (20).

$$j_1^2 + j_L\xi e^{2f\eta_2}j_1 - \xi e^{2f\eta_2}j_L^2 = 0 \tag{A16}$$

References

[1] M. Enyo, in: B.E. Conway, J.O'M. Bockris, E. Yeager, S.U. Khan, R.E. White (Eds.), Comprehensive Treatise of Electrochemistry, vol. 7, Plenum Press, New York, 1983, p. 241 (Chapter 4).
[2] M.A. Montero, M.R. Gennero de Chialvo, A.C. Chialvo, Electrochem. Commun. 12 (2010) 398.
[3] P.M. Quaino, J.L. Fernández, M.R. Gennero de Chialvo, A.C. Chialvo, J. Mol. Catal. A: Chem. 252 (2006) 156.
[4] M.R. Gennero de Chialvo, A.C. Chialvo, Phys. Chem. Chem. Phys. 6 (2004) 4009.
[5] J.X. Wang, T.E. Springer, R.R. Adzić, J. Electrochem. Soc. 153 (2006) A1732.
[6] S. Chen, A. Kucernak, J. Phys. Chem. B 108 (2004) 13984.
[7] M.D. Arce, J.L. Fernández, M.R. Gennero de Chialvo, A.C. Chialvo, J. Electroanal. Chem. 642 (2010) 41.
[8] P.M. Quaino, M.R. Gennero de Chialvo, A.C. Chialvo, Electrochim. Acta 52 (2007) 7396.
[9] M.R. Gennero de Chialvo, A.C. Chialvo, Curr. Top. Electrochem. 11 (2006) 1.
[10] L.B. Anderson, C.N. Reilley, J. Electroanal. Chem. 10 (1965) 295.
[11] C.R. Christensen, F.C. Anson, Anal. Chem. 35 (1963) 205.
[12] D.M. Oglesby, S.H. Omang, C.N. Reilley, Anal. Chem. 37 (1965) 1312.
[13] A.J. Bard, in: A.J. Bard, M.V. Mirkin (Eds.), Scanning Electrochemical Microscopy, Marcel Dekker, New York, 2001, p. 1 (Chapter 1).
[14] M.A.G. Zevenbergen, B.L. Wolfrum, E.D. Goluch, P.S. Singh, S.G. Lemay, J. Am. Chem. Soc. 131 (2009) 11471.
[15] R.M.Q. Mello, E.A. Ticianelli, Electrochim. Acta 42 (1997) 1031.
[16] J.L. Fernández, M.R. Gennero de Chialvo, A.C. Chialvo, Phys. Chem. Chem. Phys. 5 (2003) 2875.
[17] M.R. Gennero de Chialvo, A.C. Chialvo, J. Electroanal. Chem. 415 (1996) 97.
[18] M.R. Gennero de Chialvo, A.C. Chialvo, Electrochim. Acta 44 (1998) 841.
[19] W.J. Albery, Trans. Faraday Soc. 62 (1966) 1575.
[20] J. Velmurugan, P. Sun, M.V. Mirkin, J. Phys. Chem. C 113 (2009) 459.
[21] J. Zhou, Y. Zu, A.J. Bard, J. Electroanal. Chem. 491 (2000) 22.
[22] S. Lubetkin, Electrochim. Acta 48 (2002) 357.
[23] K. Borgwarth, J. Heinze, in: A.J. Bard, M.V. Mirkin (Eds.), Scanning Electrochemical Microscopy, Marcel Dekker, New York, 2001, p. 201 (Chapter 6).
[24] X. Lu, Q. Wang, X. Liu, Anal. Chim. Acta 601 (2007) 10.
[25] K. Jambunathan, B.C. Shah, J.L. Hudson, A.C. Hillier, J. Electroanal. Chem. 500 (2001) 279.
[26] S. Jayaraman, A.C. Hillier, J. Phys. Chem. B 107 (2003) 5221.
[27] C.G. Zoski, J. Phys. Chem. B 107 (2003) 6401.
[28] A.J. Bard, F.-R.F. Fan, J. Kwak, O. Lev, Anal. Chem. 61 (1989) 132.
[29] M.V. Mirkin, T.C. Richards, A.J. Bard, J. Phys. Chem. 97 (1993) 7672.
[30] J.L. Amphlett, G. Denuault, J. Phys. Chem. B 102 (1998) 9946.
[31] C.G. Zoski, J.C. Aguilar, A.J. Bard, Anal. Chem. 75 (2003) 2959.
[32] C.G. Zoski, C.R. Luman, J.L. Fernández, A.J. Bard, Anal. Chem. 79 (2007) 4957.

Please cite this article in press as: J.L. Fernández, J. Electroanal. Chem. (2010), doi:10.1016/j.jelechem.2010.09.002